

Helix swapping between two α/β barrels: crystal structure of phosphoenolpyruvate mutase with bound Mg^{2+} -oxalate

Kui Huang¹, Zhong Li¹, Yong Jia², Debra Dunaway-Mariano² and Osnat Herzberg^{1*}

Background: Phosphonate compounds are important secondary metabolites in nature and, when linked to macromolecules in eukaryotes, they might play a role in cell signaling. The first obligatory step in the biosynthesis of phosphonates is the formation of a carbon–phosphorus bond by converting phosphoenolpyruvate (PEP) to phosphonopyruvate (P-pyr), a reaction that is catalyzed by PEP mutase. The PEP mutase functions as a tetramer and requires magnesium ions (Mg^{2+}).

Results: The crystal structure of PEP mutase from the mollusk *Mytilus edulis*, bound to the inhibitor Mg^{2+} -oxalate, has been determined using multiwavelength anomalous diffraction, exploiting the selenium absorption edge of a selenomethionine-containing protein. The structure has been refined at 1.8 Å resolution. PEP mutase adopts a modified α/β barrel fold, in which the eighth α helix projects away from the α/β barrel instead of packing against the β sheet. A tightly associated dimer is formed, such that the two eighth helices are swapped, each packing against the β sheet of the neighboring molecule. A dimer of dimers further associates into a tetramer. Mg^{2+} -oxalate is buried close to the center of the barrel, at the C-terminal ends of the β strands.

Conclusions: The tetramer observed in the crystal is likely to be physiologically relevant. Because the Mg^{2+} -oxalate is inaccessible to solvent, substrate binding and dissociation might be accompanied by conformational changes. A mechanism involving a phosphoenzyme intermediate is proposed, with Asp58 acting as the nucleophilic entity that accepts and delivers the phosphoryl group. The active-site architecture and the chemistry performed by PEP mutase are different from other α/β -barrel proteins that bind pyruvate or PEP, thus the enzyme might represent a new family of α/β -barrel proteins.

Introduction

Phosphonate compounds contain a carbon–phosphorus linkage that renders them resistant to acid-catalyzed, base-catalyzed, and phosphotransferase-catalyzed hydrolysis [1,2]. They display a wide spectrum of biological activities and have been used as antibiotics, antifungal, insecticidal, antiviral, antihypertensive, herbicidal, and neurotoxic agents. Naturally produced phosphonates span a range of secondary metabolites, such as the antibiotics fosfomicin, bialaphos and K-26, thought to assist the organisms producing them in prevailing over their environmental competitors [3–5]. In eukaryotes, phosphonates are found as adducts that are covalently linked to cellular lipids, glycolipids, and proteins. The physiological roles of the phosphonate macromolecules have not yet been established. The concentration of the phosphonates at cell surfaces, however, particularly in nervous tissue, suggests that they might be important for cell signalling [6].

The biosynthesis of phosphonates relies on an enzyme-mediated chemistry that involves intramolecular oxygen

Addresses: ¹Center for Advanced Research in Biotechnology, University of Maryland Biotechnology Institute, 9600 Gudelsky Drive, Rockville, Maryland 20850, USA and ²Department of Chemistry, University of New Mexico, Albuquerque, New Mexico 87131, USA.

*Corresponding author.
E-mail: osnat@carb.nist.gov

Key words: crystal structure, phosphoenolpyruvate mutase, phosphonates, X-ray crystallography

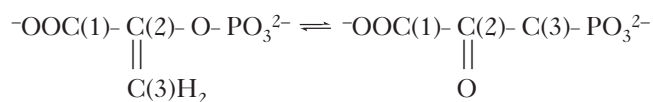
Received: 8 January 1999
Revisions requested: 9 February 1999
Revisions received: 22 February 1999
Accepted: 23 February 1999

Published: 30 April 1999

Structure May 1999, 7:539–548
<http://biomednet.com/elecref/0969212600700539>

© Elsevier Science Ltd ISSN 0969-2126

to carbon phosphoryl transfer in vinyl phosphate esters. Phosphoenolpyruvate (PEP) mutase catalyzes such chemistry [7,8]:



The P–C bond in phosphonopyruvate (P-pyr) is higher in energy than the P–O bond in PEP, thus the reaction equilibrium favors PEP formation ($K_{\text{eq}} = 2\text{--}9 \times 10^{-4}$ [9]). Despite the unfavorable solution equilibrium, the mutase functions in P-pyr synthesis driven by the coupling action of P-pyr decarboxylase. The smaller P-pyr $K_{\text{m}} = 3.5 \mu\text{M}$ compared with PEP $K_{\text{m}} = 770 \mu\text{M}$ measured for PEP mutase from *Tetrahymena pyriformis* suggests that it might bind P-pyr tighter than PEP does, thus compensating for the energy differences between substrate and product. Indeed, the steady-state turnover rate in the PEP-forming direction is 20-fold faster than that in the P-pyr-forming direction ($k_{\text{cat}} = 100 \text{ s}^{-1}$ compared with 5 s^{-1} , respectively [9]).

Mechanistic studies of the *T. pyriformis* PEP mutase have been carried out in the PEP-forming direction, with Mg^{2+} serving as the required divalent metal ion [10]. The rearrangement, $PEP \rightleftharpoons P\text{-pyr}$, is an intramolecular reaction that occurs with retention of configuration at phosphorus [11,12]. Oxalate, a pyruvate enolate analog, is a tight binding competitive inhibitor of the enzyme [13]. These findings have been taken as evidence for an associative phosphoryl transfer mechanism, which proceeds via a phosphoenzyme–pyruvate enolate intermediate, or a dissociative phosphoryl transfer reaction, which proceeds via an enzyme-bound metaphosphate–pyruvate enolate complex. Previous attempts to distinguish between these two catalytic pathways experimentally have not been successful [9]. Other mechanisms that predict the retention of configuration at phosphorus have been discussed [11]. These were considered unlikely, however, because they implied at least one intermediate with a pentacoordinated phosphorus that must undergo a pseudorotation before collapsing to product. So far, such a process has not been shown to be associated with any enzymatic reaction, and for PEP mutase it would involve an extremely unstable intermediate or an inefficient, multistep reaction.

PEP mutase and/or its encoding gene have been isolated from a number of phosphonate-producing bacteria [14–16] as well as from protozoa [8,10,17] and mollusks [9,18]. These are oligomeric proteins with subunit sizes that vary between 292 and 435 amino acids in length, with the larger subunits corresponding to a bifunctional enzyme. Amino acid sequence analysis has shown that PEP mutase belongs to a family of enzymes that includes the carboxyl PEP mutase and isocitrate lyase [13], and our recent searches using the search program BLAST [19] revealed a number of proteins to which functions have not been assigned. To date, no three-dimensional structure has been published for any of these proteins.

PEP mutase from the mollusk *Mytilus edulis*, the subject of this study, is a 33,000 Da tetrameric enzyme as indicated by gravity gel filtration chromatography and by sedimentation equilibrium. The steady-state rate constants in the direction of PEP formation were measured to be $k_{cat} = 34 \text{ s}^{-1}$ and $K_m = 3 \text{ }\mu\text{M}$ [20]. The gene encoding the enzyme was cloned and overexpressed in *Escherichia coli* and the catalytic roles of stringently conserved residues tested [18]. The crystal structure determination reported here has been undertaken in order to obtain an atomic view of the active site and to assist with the elucidation of the catalytic mechanism.

Results and discussion

Structure determination

Wild-type and selenomethionine-incorporated mussel PEP mutases were crystallized under similar conditions, with two molecules per asymmetric unit (Table 1). The

structure was determined using the multiwavelength anomalous diffraction (MAD) method [21], exploiting the selenium absorption edge of the selenomethionyl-containing protein (Table 1). The initial electron-density map at 2.0 Å resolution was of high quality and clearly revealed the positions of all but the four N-terminal amino acid residues. All 14 selenium sites of the two molecules in the asymmetric unit were visible and the density for the bound Mg^{2+} –oxalate inhibitor was unambiguous. At the end of the refinement, the working and free R factors were 0.188 and 0.256, respectively, for reflections between 8.0 and 1.8 Å for which $F \geq 2\sigma(F)$ (Table 2). The overall R factor, after adding the data reserved for free R calculation at the end of the refinement is 0.190. The root mean square (rms) deviations from ideal bond length and bond angle values of the standard geometry compiled by Engh and Huber [22] are 0.021 Å and 2.0°, respectively. The conformation of the two molecules in the asymmetric unit is nearly identical, with an rms deviation of 0.3 Å for equivalent α carbon atoms.

Monomer structure

PEP mutase packs in the crystal as a dimer of dimers. Each monomer adopts a modified version of the α/β -barrel fold (Figure 1a,b). The classic α/β barrel contains eight repeating β/α motifs that together form an eight-stranded parallel β barrel, surrounded by eight helices. In PEP mutase, however, there are only seven helices embracing the central β barrel. The eighth helix (encompassing residues 238–260) protrudes from the barrel, exposing a hydrophobic patch on

Table 1

Data collection and phasing statistics.

Space group	C222 ₁		
Unit-cell dimensions (Å)	a = 90.4; b = 131.1; c = 90.9		
No. of molecules in the asymmetric unit	2		
MAD data collection	Inflection (λ_1)	Peak (λ_2)	Remote (λ_3)
Wavelength (Å)	0.9787	0.9784	0.9500
Resolution limit (Å)	1.8	1.8	1.8
Total No. of observations	309,963	264,308	349,754
Unique reflections	49,056	48,415	53,685
Redundancy	6.3	5.5	6.5
Completeness (%) [*]			
Overall	94 (84)	92 (85)	95 (85)
1.84–1.78 Å	67 (64)	69 (61)	76 (64)
[†] R _{merge} (%)	7.3	8.2	7.0
[‡] Phasing power	–	1.09	2.26
[§] R _{miphere}			
$\Delta\lambda$ (+/–)	0.54	0.47	0.49
$\Delta(\lambda_i - \lambda_1)$	–	0.80	0.54
Figure of merit	0.72		

^{*}The values in parentheses correspond to reflections for which $I \geq 2\sigma(I)$. [†] $R_{sym} = \sum_{hkl} [(\sum_i I_i - \langle I \rangle) / \sum_i I_i]$, where $\langle I \rangle$ is the mean intensity of symmetry equivalent reflections. [‡]Phasing power – rms ($|F_H|/E$), where E is the lack of closure error.

[§] $R_{miphere} = \sum_h (|F_P + F_H(\text{calc})| - |F_{PH}|) / \sum_h (|F_{PH}| - |F_P|)$, for the anomalous differences or for the dispersive differences.

Table 2

Refinement statistics.	
Resolution range (Å)	8.0–1.8
Wavelength (Å)	0.9500
No. unique reflections ($F \geq 2\sigma(F)$)	43,980
R factor*	0.190 (0.188)
$R_{\text{free}}^{\dagger}$	0.256
Completeness (%)	
overall (8.0–1.8 Å)	88.6
1.88–1.80 Å shell	83.3
Rms deviation from ideal geometry	
bond length (Å)	0.021
bond angle (°)	2.0
Number of atoms	
protein	4549
solvent	591
oxalate	12
Mg ²⁺	2
Average B factors (Å ²)	
protein mainchain	16
protein sidechain	17
solvent	30
oxalate	14
Mg ²⁺	15

*R factor = $\sum_{\text{hkl}} |F_o - F_c| / \sum_{\text{hkl}} F_o$, where F_o and F_c are the observed and calculated structure factors, respectively. The value in parentheses corresponds to the working data set before adding the data reserved for free R calculation. [†] R_{free} is the R factor calculated for a randomly selected 10% of the reflections that were omitted from refinement.

the β sheet of the barrel. The strayed helix and the two ensuing helices (residues 272–278 and 281–291) form a tail at the C terminus that makes little contact with the barrel structure of this monomer. As is seen typically with α/β barrels, the substrate (inhibitor in this case) binds in a crevice at the center of the barrel, close to the carboxy ends of the β strands [23].

Helix swapping between monomers

Two PEP mutase molecules are closely associated across a crystallographic twofold symmetry axis along the b unit cell axis (Figure 1c). The strayed helix of one monomer packs against the β sheet's exposed hydrophobic region of the second monomer, and vice versa. Thus, the swapped helices form two complete α/β barrels, and also mediate the tight dimeric association. The two C-terminal helices ensuing from the strayed helix in one monomer traverse the barrel of the neighboring monomer across its active site, furthering the intertwined dimer association. The helix swapping results in an extensive dimer interface, characterized by both hydrophobic and hydrogen-bond interactions. A total of 5672 Å² molecular surface area is buried at this interface. Domain swapping has been observed in a number of proteins and is thought to provide a mechanism for oligomeric assembly [24]. To the best of our knowledge, the dimer association in PEP mutase is the first example of swapped helices in α/β barrel structures.

Tetramer formation

The association of monomers across a noncrystallographic twofold symmetry axis that runs approximately parallel to the c unit cell axis leads to tetramer formation (Figure 1d). Two dimers, each with swapped helices, form the tetramer, giving rise to two additional subunit–subunit interfaces. One interface is rather unusual because it is largely governed by salt bridges (Figure 1e). The total molecular surface area buried at this interface is 1607 Å². The ion pairs are Glu72–Arg106, Asp76–Lys102, and Glu283–Arg97, and the twofold symmetry axis leads to a total of six salt bridges. A pair of tight electrostatic interactions between the carboxylate group of Asp147 and the hydroxyl group of Tyr291 (2.5 Å) are also present. The eight residues involved in the above interactions are invariant in PEP mutase from *T. pyriformis*, but they are not conserved among all known amino acid sequences of PEP mutase. The second interface is generated by the crystallographic twofold symmetry axis along the a unit cell axis, as shown in Figure 1d. This interface buries only 951 Å² molecular surface area. Six hydrogen bonds are formed, from Asn60 O to Asn95 N^{δ2}, Glu61 O^{ε2} to Asn94 N^{δ2} and S63 O γ to Thr65 O γ , and vice versa. These residues are conserved among PEP mutases from *M. edulis* [18], *T. pyriformis* and *Streptomyces hygrosopicus* [14], but not in the enzyme from *Streptomyces wedmorensis* [15].

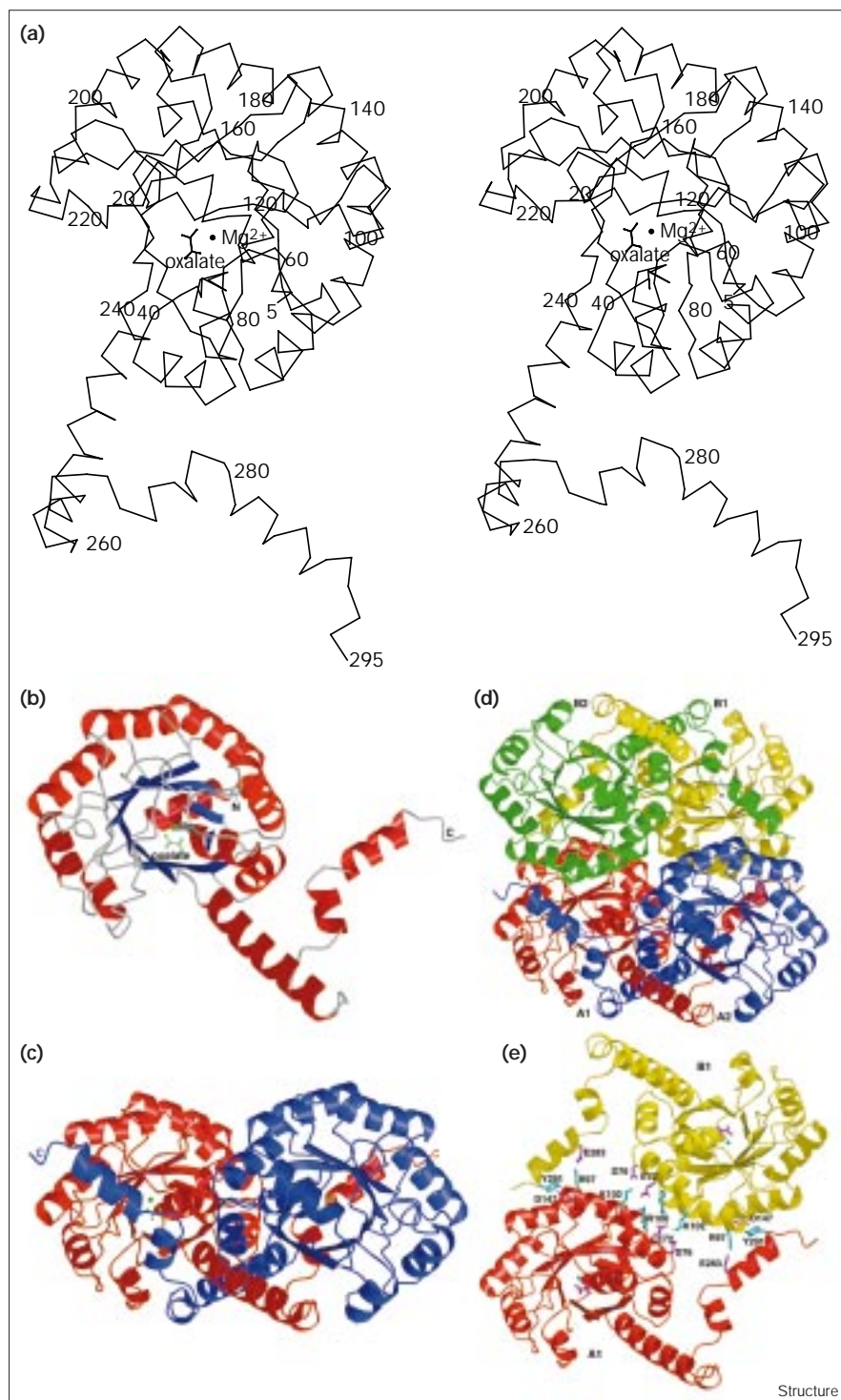
PEP mutase from mollusk forms a tetramer in solution. It is likely that the tetramer observed in the crystal resembles the tetrameric association under physiological conditions. In particular, the dimer formed by the two monomers that swap helices seems relevant because of the intertwined nature of the interactions.

Binding of Mg²⁺ and oxalate

The inhibitor binds with the two carboxylate groups of oxalate coordinating to Mg²⁺, which in turn interacts with three water molecules and with the carboxylate group of Asp85 (Figure 2a). Each of the water molecules (Wat 1–3) interacts with a charged amino acid (Wat1 with Glu144, Wat2 with Asp87, and Wat3 with Lys120 and Asp58). The Mg²⁺ ligands are arranged in an octahedral geometry with cation–ligand distances of 2.2–2.3 Å (Figure 2b). Oxalate–protein interactions occur with Arg159 N^{η2} (2.6 Å), Trp44 N^{ε1} (3.0 Å), Ser46 O γ (2.6 Å), and with an oxyanion hole formed by the mainchain nitrogen atoms of Gly47 and Leu48 (3.2 Å and 2.8 Å, respectively). Gly47 and Leu48 are located at the N terminus of a short helix (encompassing residues 46–54), thus the helix dipole might provide additional favorable interaction with the negatively charged oxalate.

The active site of PEP mutase is inaccessible from either end of the α/β barrel. The bottom of the barrel (N-terminal ends of the β strands) is blocked by an N-terminal α helix (Figure 1a,b). The top of the barrel (the C-terminal

Figure 1



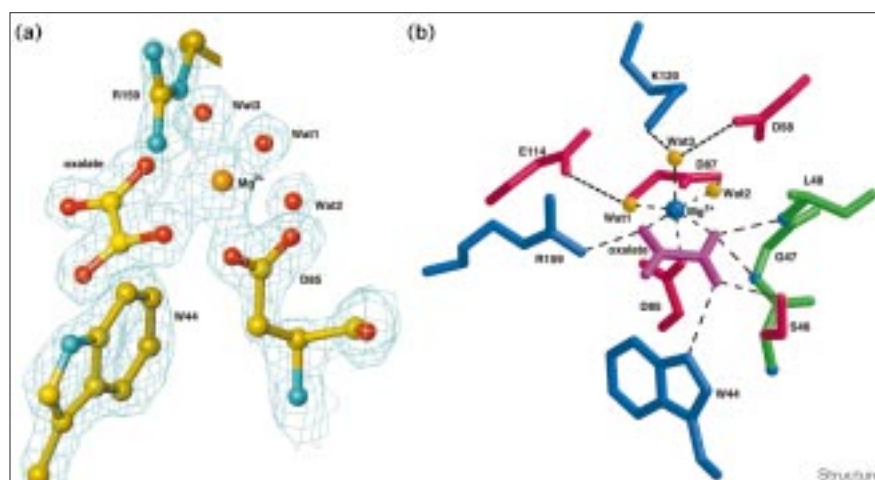
Monomer, dimer and tetramer structures of PEP mutase from *Mytilus edulis*. The figure was generated with the program MolScript [50], and rendered with Raster3D [51], using the 2.0 version [52] and a TCL-TK front-end developed by Hillary Gilson (personal communication). (a) Stereoscopic representation of the α carbon atom trace of the PEP mutase monomer. Every 20th residue is labeled, as well as the oxalate and Mg^{2+} . (b) Ribbon representation of the monomer. The α helices and β strands are shown in red and blue, respectively. Bound Mg^{2+} and oxalate are shown in green. The N and C termini are labeled. (c) Dimer formation by helix swapping. The two monomers are colored in red and blue. Bound Mg^{2+} and oxalate are shown in green. (d) The tetramer. Monomers A1 (in red) and A2 (in blue) shuffle helices, as do monomers B1 (yellow) and B2 (green). Bound Mg^{2+} and oxalate are colored in magenta. (e) Salt-bridge interactions between two monomers in the crystal asymmetric unit. The two monomers correspond to monomers A1 and B1 of the tetramer. Negatively and positively charged residues are colored magenta and cyan, respectively.

ends of the β strands) is capped by sidechains of residues 120–124 located on a 20-residue loop (Figure 1a), and by the C-terminal helical segment of the neighboring molecule (Figure 1c). N-terminal ends of α/β barrels are usually blocked, as the action takes place at the C-terminal

end of the β sheet. Thus, if PEP mutase exists in solution in the associated form with the swapped helices, ligand binding and dissociation must be accompanied by conformational changes of the capping surface loop and/or the traversing helical segment.

Figure 2

Mg²⁺ and oxalate binding to PEP mutase. (a) Electron density associated with Mg²⁺, oxalate, three solvent molecules (Wat1, Wat2 and Wat3), and several protein residues. The coefficients $2F_o - F_c$ and calculated phases are used (where F_o and F_c are the observed and calculated structure-factor amplitudes), and the map is contoured at the 2.0σ level. (b) Interactions of Mg²⁺ and oxalate with PEP mutase. The interactions of the three bridging water molecules with protein residues are also shown.



Catalytic residues

The Mg²⁺-binding residue Asp85 and the oxalate-binding residues Ser46 and Arg159 are invariant among the four PEP mutases that have been sequenced so far. Other invariant residues in which sidechains are located in close proximity to the Mg²⁺-oxalate are Asp58, Asp87, Glu114 and Lys120 (Figure 2b). These four residues interact with three water molecules, which in turn interact with Mg²⁺. Mutagenesis studies have shown that Asp58 is essential for catalysis [18]. When replaced by an alanine residue, activity is abolished despite the fact that in the current crystal structure Asp58 is not in direct contact with Mg²⁺ or with oxalate. Glu114 and Arg159 are important for substrate binding and catalysis, although residual activity was detected when these positions were mutated. The E114A and R159K enzymes displayed 19–73-fold increased K_m values, and 3×10^3 – 10^4 -fold reduced k_{cat} values toward PEP formation compared with wild-type PEP mutase. Preliminary experiments with R159A showed that this variant retained some activity as well. Asp87 and Lys120 are also important for catalysis, with k_{cat} values for the D87A and K120R mutants being 0.5% and 0.9% of the value for the wild-type enzyme, respectively.

Catalytic mechanism

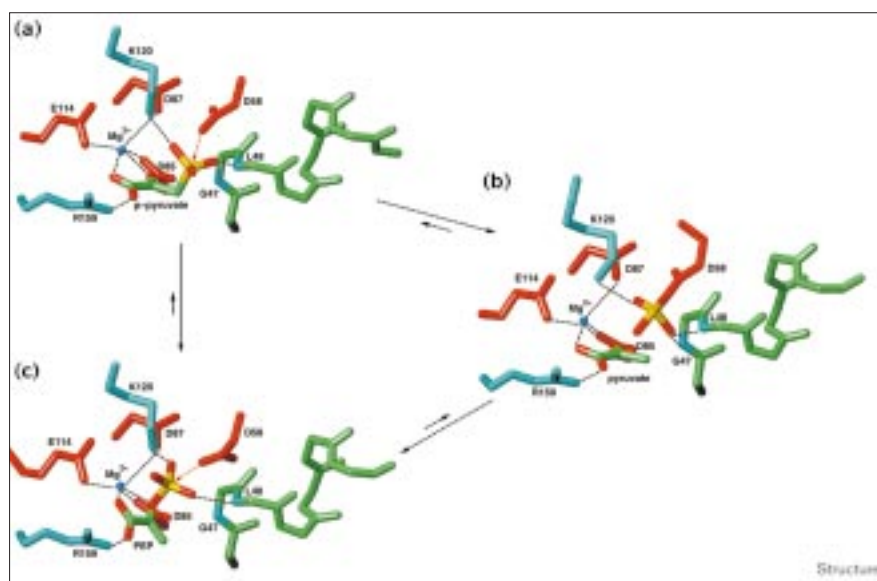
Inspection of the PEP mutase–oxalate structure and attempts to model the binding modes of PEP and P-pyr indicate that two alternative binding modes of the substrate and the metal ion must be considered. The first model positions the phosphoryl group on the side of Arg159. The associative mechanism involving the phosphoenzyme intermediate cannot be represented by this mode of binding because there is no precedent for an arginine as a phospho-carrier residue. The dissociative mechanism involving metaphosphate might be considered with skepticism, because there has been no proven example of such

phosphoryl transfer mechanism in biological processes. Also, the residual activity detected with the R159A mutant enzyme indicates that Arg159 is not as important as Asp58. Nevertheless, PEP or P-pyr might occupy the position of the oxalate, with the enol group replacing the Arg159-interacting carboxylate group of oxalate, and the phosphoryl group forming an ion pair with Arg159 (model not shown). Mg²⁺ remains in the same site as seen in the crystal structure. Although the environment of the phosphoryl group is quite crowded, there is space to accommodate the substrate in this manner. As the phosphoryl group is transferred, the metaphosphate can still form an ionic interaction with the guanidinium group of Arg159.

A plausible associative mechanism that utilizes a phosphoenzyme intermediate invokes Asp58 as the phospho-carrier residue (Figure 3). An in-line attack of the carboxylate group of Asp58 on phosphorous is associated with two transition states, each with a pentagonally coordinated phosphorous. One transition state corresponds to accepting the phosphoryl group from P-pyr, and the other corresponds to delivering the phosphoryl group to form PEP. A phospho-aspartate intermediate is not unprecedented in biological systems. A number of examples have been documented, including sarcoplasmic reticulum ATPase [25], CheY [26], human phosphomannomutase, and L-3-phosphoserine phosphatase [27].

For the phosphoryl group to be transferred to Asp58, it must be located on the side of the oxalate's carboxylate group that interacts with the oxyanion hole (formed by the mainchain amide groups of Gly47 and Leu48). Moreover, if the enol group of pyruvate simply replaces this carboxylate group of oxalate, there is no space to accommodate the phosphoryl group of PEP or P-pyr and Asp58 is too far away to accept and deliver a phosphoryl group.

Figure 3



Proposed associative phosphoenzyme intermediate mechanism of PEP mutase. Possible electrostatic interactions are shown as broken lines. (a) Mg^{2+} -P-pyr-enzyme active site. (b) Mg^{2+} -pyruvate-phosphoenzyme. (c) Mg^{2+} -PEP-enzyme active site.

Thus a shift of the pyruvate moiety toward Asp58 is required, concomitantly with a shift of Mg^{2+} to the site of Wat1. Consequently, the metal interacts directly with three protein carboxylate groups, Asp85, Asp87 and Glu144, instead of the one carboxylate group and three water molecules seen in the oxalate-bound structure. In fact, Mg^{2+} is usually seen interacting with a number of carboxylate groups, whereas Mg^{2+} that uses three water molecules as 'fillers' to bridge to the protein is unusual. This might yet be another case of an inhibitor-binding mode that differs from that of a true substrate. The arrangement seen in the PEP mutase- Mg^{2+} -oxalate complex might have arisen for optimal interactions between the protein and both carboxylate groups of oxalate.

The invariant Asp58 is located on a loop flanked by two helices at the top of the α/β barrel (residues 46–54 and residues 64–76). Its carboxyl group interacts with Wat1 and Wat3, which in turn coordinate to Mg^{2+} . In the model of the PEP mutase-P-pyr complex (Figure 3a), Asp58 O^{E1} is located 2.0 Å away from phosphorus of P-pyr, ready for in-line nucleophilic attack. The phosphoryl group forms electrostatic interactions with the oxyanion hole and with Lys120 N^ζ. The carboxyl group of P-pyr forms an ion pair with Arg159. By coordinating to both the enzyme and P-pyr, Mg^{2+} assists with precise positioning of the substrate for phosphotransfer to take place.

Several interactions stabilize the phosphoenzyme intermediate after the phosphoryl group is transferred to Asp58 (Figure 3b). These include an ion-pair interaction with the amino group of Lys120, and electrostatic interactions with the oxyanion hole and the ensuing helix dipole. Pyruvate

remains coordinated to Mg^{2+} , and the ion-pair interaction with Arg159 is maintained. A rotation of the Asp58 sidechain and a slight adjustment of pyruvate might be associated with the delivery of the phosphoryl group back to pyruvate to obtain PEP (Figure 3c). The interaction of the phosphoryl group with Lys120 and the oxyanion hole is maintained, although not precisely as modeled in P-pyr.

A couple of cautionary comments seem appropriate here. First, rationalizing the stronger binding of the enzyme to P-pyr than to PEP in terms of the details of the models is deemed futile. These are only approximate models that are insufficient for such conjecture. The structural basis for the preferred binding of P-pyr over PEP remains unknown, as does the question of how the product can diffuse in and out of a blocked active site. These issues might be answered by obtaining the crystal structure of a true enzyme-substrate complex. Second, the binding mode depicted in Figure 3 is also consistent with a dissociative mechanism regardless of our reluctance to invoke it in a biological process. With the structure at hand, experiments could be designed to increase the lifetime and trap the postulated phosphoenzyme adduct, and thus resolve the two alternative mechanisms.

Comparison with other α/β -barrel structures

The numerous enzymes that adopt the α/β -barrel structure exhibit diverse functions and are not necessarily related to each other by amino acid sequence homology criteria. This visually appealing fold has attracted much discussion about the possibility for a single ancestor protein of all α/β -barrel proteins. Farber and Petsko [28] argued in favor of such common ancestor although they

did recognize the lack of evidence in support of this hypothesis. Packing analysis of the interior of the sheet in α/β barrels led Lesk *et al.* [29] to the conclusion that there are at least two different ancestral proteins because there are two conflicting ways of packing sidechains in the center of the barrel. The discrepancy between these packing modes is reconciled, however, when the possibility of circular permutation of the gene is considered. The current SCOP classification database [30] differentiates between 18 α/β -barrel superfamilies, where members of a superfamily are considered evolutionarily related, but need not show significant sequence homology or identical function (although they usually share some similar aspects of function). PEP mutase does not exhibit significant sequence homology with any of the α/β -barrel proteins. Does it belong to a known superfamily?

The program DALI [31] was used to identify α/β barrels related to PEP mutase. The long list contains three enzymes of which structures have been determined in the presence of pyruvate or PEP, each representing a different superfamily. *N*-acetylneuraminase lyase ([32], PDB entry 1nal) aligns best with PEP mutase, with an rms deviation of 2.1 Å for 172 α carbon atom pairs (using the superposition tool of the program O [33]). The enzyme catalyzes the cleavage of sialic acid to pyruvate and *N*-acetyl-D-mannosamine. *N*-acetylneuraminase lyase is a member of an enzyme superfamily that utilizes a Schiff-base formation to form a lysine-substrate intermediate. No significant amino acid sequence similarity exists between PEP mutase and any member of that superfamily. The structure of *N*-acetylneuraminase lyase with a pyruvate forming a Schiff base has been determined ([34], PDB entry code 1fdy). The alignment with PEP mutase reveals that although the overall fold of the α/β barrels is similar (except that the barrel of *N*-acetylneuraminase lyase is complete as a monomer), there is little resemblance between the active sites (Figure 4). One common feature is the similar location of an oxyanion hole that stabilizes the carboxylate group of the substrate or inhibitor. Note though, that for the proposed associative pathway in PEP mutase, it is the phosphoryl group that should be located in the oxyanion hole and not the carboxylate group. In addition, the superposition shows that Arg159 in PEP mutase is located in an equivalent position to Tyr137 in *N*-acetylneuraminase lyase, a residue that is implicated in catalysis. Overall though, the location of catalytic residues is sufficiently different and the chemistry performed by the two enzymes is completely unrelated, supporting the notion that PEP mutase is not a member of the superfamily.

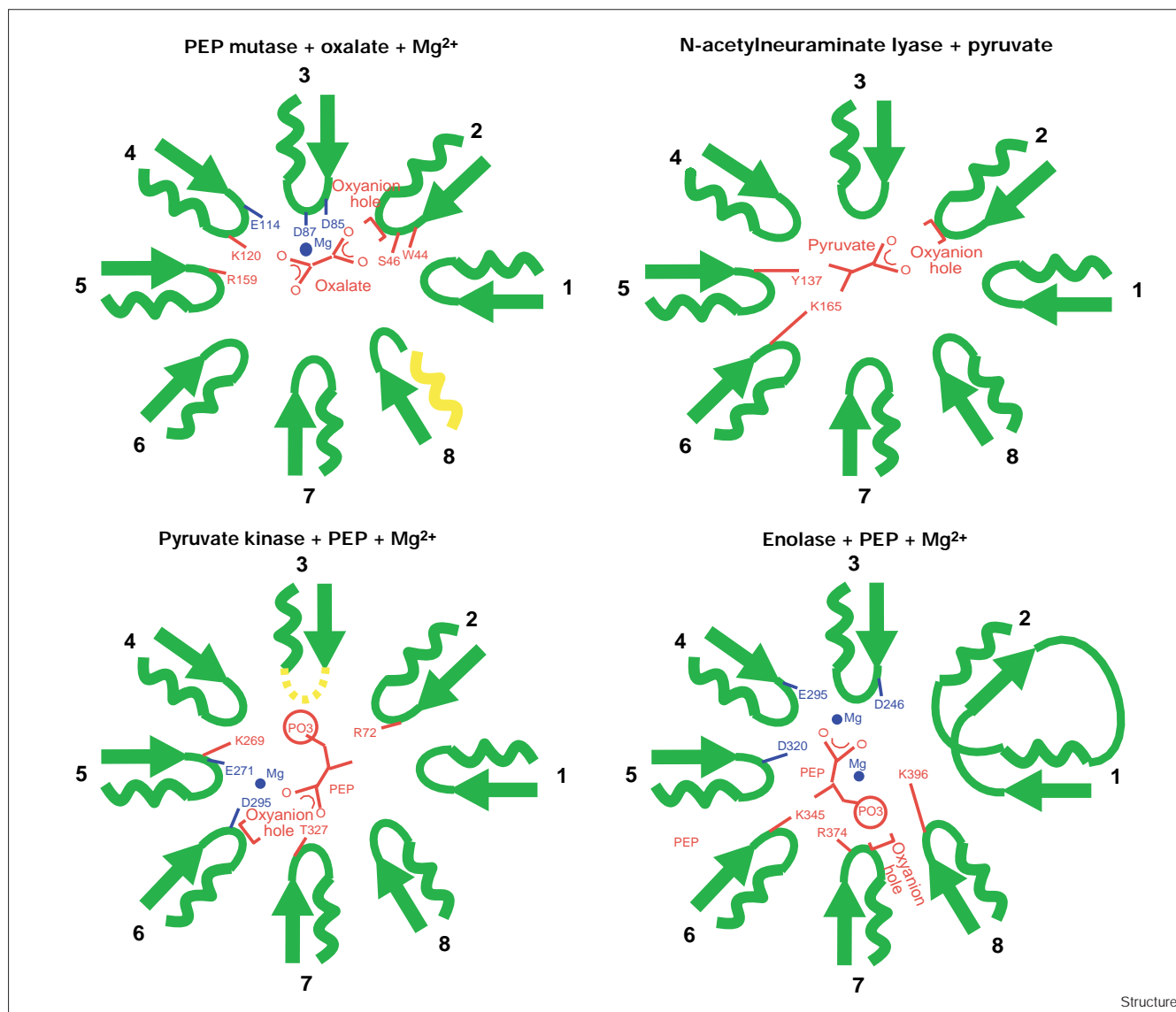
The second structure that has been examined is that of pyruvate kinase complexed with Mg^{2+} -PEP ([35], PDB entry code 1aqf). The superposition on PEP mutase resulted in an rms deviation of 2.4 Å for 154 equivalent α -carbon atoms. Pyruvate kinase catalyzes the intermolecular

phosphoryl transfer from PEP to ADP in the presence of Mg^{2+} . Despite the common substrate and the use of charged residues and an oxyanion hole to complement charged groups of the substrates, there is little resemblance between the binding modes (Figure 4). Different β/α units are involved in binding to PEP-oxalate and to Mg^{2+} . The location of the oxyanion hole is also different. Common to both enzymes, the side face of pyruvate-oxalate interacts with Mg^{2+} , with the cation coplanar with the ligand. In our view, these attributes are not sufficient to classify PEP mutase as a member of the pyruvate kinase family.

The third example is that of enolase ([36,37], PDB entry codes 1one and 2one). The enzyme catalyzes the reversible conversion of PEP to 2-phospho-D-glycerate (PGA), a reaction that does not involve a phosphoryl transfer. For one structure, 1one, the interpretation of the electron-density map was that every active site of the dimeric protein contains two Mg^{2+} ions, and PEP and PGA, each with half occupancy. For the second structure, 2one, one molecule of the dimer contains PEP and a single Mg^{2+} , and the second molecule contains PGA and two cations, Mg^{2+} and Li^+ . The superposition of enolase with PEP mutase resulted in an rms deviation of 2.1 Å for 118 equivalent α -carbon atoms. The lower number of superpositioned atom pairs compared with the preceding superpositions can be attributed to the departure of the enolase α/β barrel from the classical barrel architecture. The topology of the first two β/α units is $\beta,\beta,\alpha,\alpha$. The active-site architectures of PEP mutase and enolase exhibit no striking resemblance, except for the general observation that charge-charge interactions govern binding, an obvious feature given that PEP and Mg^{2+} are charged entities (Figure 4). The β/α motifs involved in interactions with substrates and cations are different in PEP mutase and enolase. An oxyanion hole in enolase interacts with the phosphoryl group (as we propose for the associative pathway mechanism in PEP mutase), but it is formed by a residue on the loop of the seventh β/α unit and by two mainchain nitrogen atoms on a non-barrel segment at the N terminus of the molecule (Figure 4). The Mg^{2+} common to both 1one and 2one coordinate sets interacts with three protein carboxylate groups and with the carboxylate group of the pyruvate moiety. The interaction with pyruvate of this Mg^{2+} does not resemble that seen in PEP mutase or pyruvate kinase. The second cation (Mg^{2+} in 1one, Li^+ in 2one) does not interact with the protein but binds to the PEP through the phosphoryl group and an oxygen atom of the carboxylate group, a mode of interaction similar to that seen in pyruvate kinase and PEP mutase.

The conclusion reached from the above comparisons is that there is no compelling evidence for an evolutionary link between PEP mutase and the other three α/β -barrel

Figure 4



Cartoon representation of ligand binding to four α/β -barrel PEP/pyruvate-utilizing enzymes. The β/α motifs are numbered sequentially. For PEP mutase, helix 8 is colored yellow because it is contributed by a neighboring molecule. The loop connecting the β/α motif 3 in pyruvate kinase corresponds to a whole domain and is

shown as a broken yellow line. Motifs 1 and 2 in enolase do not obey the classical topology of β/α motifs. Residues that interact with PEP/pyruvate/oxalate are colored red. Residues that interact with Mg^{2+} are colored blue.

PEP-utilizing proteins, thus PEP mutase might be a member of a new α/β -barrel superfamily. On the other hand, sequence homology indicates an evolutionary relationship between PEP mutase and isocitrate lyase, an enzyme with a different function but that employs related chemistry [13]. The structure of isocitrate lyase has not yet been determined. Revisiting the sequence relationship with the structure of PEP mutase at hand, the proposal for an evolutionary link between the two enzymes is strengthened because all key active-site residues are invariant in isocitrate lyase. It is therefore reasonable to

assume that the structure of isocitrate lyase is closely related to that of PEP mutase.

Biological implications

PEP mutase catalyzes the conversion of PEP to P-pyr, the key phosphorus-carbon bond-forming step of the biosynthetic pathways leading to phosphonate natural products. Stereochemical studies of this magnesium-dependent reaction indicate that a stepwise mechanism is involved, with either a phosphoenzyme intermediate or a metaphosphate and pyruvate enolate intermediate. The

exact mechanism, however, is not well understood. The key residues have been highlighted by the current structural work and accompanying mutagenesis studies. The crystal structure of the enzyme with bound Mg^{2+} -oxalate inhibitor reveals the active site architecture at the center top of an α/β barrel, with several invariant carboxylate sidechains, an invariant arginine, and the N-terminal amide nitrogens of a helix directly interacting with the Mg^{2+} and oxalate. The carboxylate group of Asp58 does not coordinate to the Mg^{2+} , but is located in a position appropriate to accept and deliver the phosphoryl group during phosphoryl transfer. Access to the active site is blocked primarily because of an intertwined association of two molecules forming a dimer. This suggests that substrate binding and dissociation requires conformational changes of the protein, the nature of which requires further investigation.

Materials and methods

Crystallization and data collection

The gene encoding the phosphoenolpyruvate mutase from *M. edulis* has been cloned in *E. coli* [18]. For the selenomethionine protein, the gene was subcloned into the expression vector pET24a(+), and over-expressed in *E. coli* strain B834(DE3), a methionine-requiring autotroph containing the T7 RNA polymerase gene under *lac* control on the host chromosome [38]. Incorporation of the selenomethionine was confirmed by mass spectrometry.

Crystals of selenomethionine protein (~ 10 mg ml⁻¹) were obtained at room temperature by vapor diffusion in hanging drops. The reservoir solution contained 15–25% w/v PEG 4000, 5% 2-propanol, 5 mM $MgCl_2$, 5 mM sodium oxalate, 5 mM DTT and 100 mM HEPES buffer at pH 7.5. The crystallization was done in a nitrogen-containing glove-box. The crystals belong to space group C222₁ with unit cell dimensions $a = 90.4$ Å, $b = 131.1$ Å, and $c = 90.9$ Å (Table 1). There are two molecules per asymmetric unit and the solvent content is 42%.

MAD data were collected at the X12C beamline of the National Synchrotron Light Source (Brookhaven National Laboratory, Upton, NY). A single crystal was flash-frozen (Oxford Cryosystem). Diffraction intensities to 1.8 Å resolution were recorded on a CCD-based detector (1K Brandeis). The crystal was orientated such that Bijvoet pairs were collected on the same image, scanning 180° in oscillation steps of 1°. Data acquisition was controlled with the computer program MADNES [39], driven by a graphical user interface [40]. Measurements were taken at three wavelengths, corresponding to the selenium's K absorption edge inflection point (λ_1), peak (λ_2), and a remote high energy point (λ_3) (Table 1). The data were processed and scaled with the computer program package HKL [41], treating Bijvoet pairs as independent measurements (Table 1).

Structure determination and refinement

The multiwavelength data were treated as arising from a multiple isomorphous replacement experiment [42]. The data measured at wavelength λ_1 were chosen as the 'native' set, whereas the data sets at λ_2 and λ_3 were treated as 'derivatives with anomalous scattering'. There are 14 selenomethionine residues in the asymmetric unit of the PEP mutase crystal. Using the anomalous differences ($\Delta F_{+/-}$) observed at λ_2 , 11 of the selenium sites were identified by Patterson superposition minimum function (SHELX [43]) and later, after structure determination, also by the program SOLVE written by Terwilliger, which uses an automatic Patterson interpretation described previously [44]. The dispersive differences ($\Delta F(\lambda_3 - \lambda_1)$) yielded the same 11 sites as those derived from the anomalous differences at λ_2 . The remaining three

sites were identified from a difference Fourier map, using the phases derived from the 11 sites.

Next, a number of programs were used as implemented in the CCP4 suite [45]. The positions, isotropic temperature factors, and the dispersive and anomalous occupancy values of the selenium scatterers were refined and phases were calculated at 2.0 Å resolution (using MLPHARE [46]). The phases were further improved by solvent flattening and histogram matching with the program DM [47]. The resulting electron-density map was readily interpretable. Model building was performed using the computer graphics program O [33].

The structure was refined using the data collected at λ_3 , which is the most complete data, measured with the highest redundancy and with the lowest R_{merge} value (Table 1). The two molecules in the crystal asymmetric unit were refined independently. Reflections between 8–1.8 Å resolution for which $F \geq 2\sigma(F)$ were included in the refinement. The program X-PLOR [48] was employed, first using the simulated-annealing protocol, and then alternating positional and isotropic temperature factor refinement cycles. Progress was monitored by the behavior of 10% of the reflections that were omitted from the refinement [49] and by inspections of the electron-density maps. For the last cycle of refinement the data reserved for free R calculation was added to the working set. The refinement statistics are shown in Table 2.

Models of bound substrates

PEP and P-pyr were positioned in the active site using the interactive computer graphics package QUANTA. Two modes of binding have been modeled. The first mode corresponds to replacing the oxalate molecule by the pyruvate moiety so that the phosphoryl group is positioned close to Arg159 and Mg^{2+} remains as seen in the crystal structure. The second mode of binding positions the phosphoryl group close to Asp58. In this orientation the pyruvate moiety and Mg^{2+} must be shifted in order to avoid a clash between the phosphoryl group and residues 46–48.

Accession numbers

The atomic coordinates have been deposited in the Brookhaven Protein Data Bank with accession code 1p6gm.

Acknowledgements

We thank Robert Sweet and John Skinner for help and advice during data collection at the National Synchrotron Light Source at Brookhaven, and Ed Eisenstein at CARB for the ultracentrifuge analysis. This work was supported by National Science Foundation Grant MCB9316934 (OH), and National Institute of Health Grant GM28688 (DDM).

References

- Hildebrand, R.L. (1983). *The Role of Phosphonates in Living Systems*. CRC Press, Inc. Boca Raton, FL.
- Mastalerz, P. (1984). In *Natural Products Chemistry* (Zalweski, R.I. & Skolik, J.J. eds), pp 171-184, Elsevier, Amsterdam.
- Kahan, F.M., Kahan, J.S., Cassidy, P.J. & Kropp, H. (1974). The mechanism of action of fosfomycin (phosphonomycin). *Ann. NY Acad. Sci.* **235**, 364-386.
- Seto, H. (1995). Biosynthesis of natural C-P compounds, phosphinotrium and biolaphos. In *Progress and Prospects of Organophosphorus Agrochemicals* (Ero, M & Casida, E., eds), pp 179-190, Kyushu University Press.
- Yamato, M., Koguchi, T., Okachi, R., Yamada, K., Nakayama, K., Kase (1986). K-26, a novel inhibitor of angiotensin I converting enzyme produced by an actinomycete K-26. *J. Antibiot.* **39**, 44-52.
- Abe, S., Araki, S., Satake, M., Fujiwara, N., Kon, K. & Ando, S. (1991). Structure of triphosphoglycosphingolipid containing N-acetylgalactosamine 6-o-2-aminoethylphosphonate in the nervous system of *Aplysia kurodai*. *J. Biol. Chem.* **266**, 9939-9943.
- Bowman, E.D., McQueney, M.S., Barry, R.J. & Dunaway-Mariano, D. (1988). Catalysis and thermodynamics of the phosphoenolpyruvate/phosphonopyruvate rearrangement. Entry into the phosphate class of naturally occurring organophosphorus compounds. *J. Am. Chem. Soc.* **110**, 5575-5576.

8. Seidel, H.M., Freeman, S., Seto, H. & Knowles, J.R. (1988). Phosphonate biosynthesis: isolation of the enzyme responsible for the formation of a carbon-phosphorus bond. *Nature* **335**, 457-458.
9. Kim, J. & Dunaway-Mariano, D. (1996). Phosphoenolpyruvate mutase catalysis of phosphoryl transfer in phosphoenolpyruvate: kinetics and mechanism of phosphorus-carbon bond formation. *Biochemistry* **35**, 4628-4635.
10. Bowman, E.D., McQueney, M.S., Scholten, J.D. & Dunaway-Mariano, D. (1990). Purification and characterization of the *Tetrahymena pyriformis* P-C bond forming enzyme phosphoenolpyruvate phosphomutase. *Biochemistry* **29**, 7059-7063.
11. Seidel, H.M., Freeman, S., Schwalbe, C.H. & Knowles, J.R. (1990). Phosphonate biosynthesis: the stereochemical course of phosphoenolpyruvate mutase. *J. Am. Chem. Soc.* **112**, 8149-8155.
12. McQueney, M.S., Lee, S-L., Swartz, W.H., Ammon, H.L., Mariano, S.M. & Dunaway-Mariano, D. (1991). Evidence for the intramolecular stepwise reaction pathway for PEP phosphomutase catalyzed P-C bond formation. *J. Org. Chem.* **56**, 7121-7130.
13. Seidel, H.M. & Knowles, J.R. (1994). Interaction of inhibitors with phosphoenolpyruvate mutase: implications for the reaction mechanism and the nature of the active site. *Biochemistry* **33**, 5641-5646.
14. Hidaka, T., Hidaka, M. & Seto, H. (1992). Studies on the biosynthesis of bialaphos (SF-1293). 14. Nucleotide sequence of phosphoenolpyruvate phosphomutase gene isolated from a bialaphos producing organism, *Streptomyces hygrosopicus*, and its expression in *Streptomyces lividans*. *J. Antibiot.* **45**, 1977-1980.
15. Hidaka, T., Goda, M., Kuzuyama, T., Takei, N., Hidaka, M. & Seto, H. (1995). Cloning and nucleotide sequence of fosfomycin biosynthetic genes of *Streptomyces wedmorensis*. *Mol. Gen. Genet.* **249**, 274-280.
16. Nakashita, H., Shimazu, A., Hidaka, T. & Seto, H. (1992). Purification and characterization of phosphoenolpyruvate phosphomutase from *Pseudomonas gladioli* B-1. *J. Bacteriol.* **174**, 6857-6861.
17. Seidel, H.M., Pompliano, D.L. & Knowles, J.R. (1992). Phosphonate biosynthesis: molecular cloning of the gene for phosphoenolpyruvate mutase from *Tetrahymena pyriformis* and overexpression of the gene product in *Escherichia coli*. *Biochemistry* **31**, 2598-2608.
18. Jia, Y. (1998). Ph.D thesis, University of Maryland at College Park, Maryland, USA.
19. Altschul, S.F., Gish, W., Miller, W., Myers, E.W. & Lipman, D.J. (1990). Basic local alignment search tool. *J. Mol. Biol.* **215**, 403-410.
20. Kim, A., Kim, J., Martin, B.M. & Dunaway-Mariano, D. (1998). Isolation and characterization of the phosphorus-carbon bond forming enzyme phosphoenolpyruvate mutase from the mollusk *Mytilus edulis*. *J. Biol. Chem.* **273**, 4443-4448.
21. Hendrickson, W.A. (1985). Analysis of protein structure from diffraction measurement at multiple wavelengths. *Trans. Am. Crystallogr. Assoc.* **25**, 11-21.
22. Engh, R.A. & Huber, R. (1991). Accurate bond and angle parameters for X-ray protein structure refinement. *Acta Crystallogr. A* **47**, 392-400.
23. Brändén, C-I. (1980). Relation between structure and function of α/β -proteins. *Q. Rev. Biophys.* **13**, 317-338.
24. Bennett, M.J., Schlunegger, M.P. & Eisenberg, D. (1994). 3D domain swapping: a mechanism for oligomer assembly. *Proteins* **4**, 2455-2468.
25. Webb, M.R. & Trentham, D.R. (1981). The stereochemical courses of phosphoric residue transfer catalyzed by sarcoplasmic reticulum ATPase. *J. Biol. Chem.* **256**, 4884-4887.
26. Sanders, D.A., Gillece-Castro, B.L., Stock, A.M., Burlingame, A.L. & Koshland, D.E. Jr. (1989). Identification of the site of phosphorylation of the chemotaxis response regulator protein, CheY. *J. Biol. Chem.* **264**, 21770-21778.
27. Collet, J.F., Stroobant, V., Pirard, M., Delpierre, G. & Van Schaffingen, E. (1998). A new class of phosphotransferase phosphorylated on an aspartate residue in an amino-terminal DXDX(T/V) motif. *J. Biol. Chem.* **273**, 14107-14112.
28. Farber, G.K. & Petsko, G.A. (1990). The evolution of α/β barrel enzymes. *Trends Biochem. Sci.* **15**, 228-234.
29. Lesk, A.M., Brändén, C-I. & Chothia, C. (1989). Structural principles of α/β barrel proteins: the packing of the interior of the sheet. *Proteins* **5**, 139-148.
30. Murzin, A.G., Brenner, S.E., Hubbard, T. & Chothia, C. (1995). SCOP: structural classification of proteins database for the investigation of sequences and structures. *J. Mol. Biol.* **247**, 536-540.
31. Holm, L. & Sander, C. (1993). Protein structure comparison by alignment of distance matrices. *J. Mol. Biol.* **233**, 123-138.
32. Izard, T., Lawrence, M.C., Malby, R.L., Lilley, G.G. & Colman, P.M. (1994). The three dimensional structure of *N*-acetylneuraminase lyase from *Escherichia coli*. *Structure* **2**, 361-369.
33. Jones, T.A., Zou, J-Y., Cowan, S.W. & Kjeldgaard, M. (1991). Improved methods for building protein models in electron density maps and the location of errors in these models. *Acta Crystallogr. A* **47**, 110-119.
34. Lawrence, M.C., Barbosa, J.A., Smith, B.J., Hall, N.E., Pilling, P.A., Ooi, H.C. & Marcuccio, S.M. (1997). Structure and mechanism of a sub-family of enzymes related to *N*-acetylneuraminase lyase. *J. Mol. Biol.* **266**, 381-399.
35. Larsen, T.M., Benning, M.M., Wesenberg, G.E., Rayment, I. & Reed, G.H. (1997). Ligand-induced domain movement in pyruvate kinase: structure of the enzyme from rabbit muscle with Mg^{2+} , K^+ , and L -phospholactate at 2.7Å resolution. *Arch. Biochem. Biophys.* **345**, 199-206.
36. Larsen, T.M., Wedekind, J.E., Rayment, I. & Reed, G.H. (1996). A carboxylate oxygen of the substrate bridges the magnesium ions at the active site of enolase: structure of the yeast enzyme complexed with the equilibrium mixture of 2-phosphoglycerate and phosphoenolpyruvate at 1.8Å resolution. *Biochemistry* **35**, 4349-4358.
37. Zhang, E., Brewer, J.M., Minor, W., Carreira, L.A. & Lebioda, L. (1997). Mechanism of enolase: the crystal structure of asymmetric dimer enolase-2-phospho-D-glycerate/enolase-phosphoenolpyruvate at 2.0 Å resolution. *Biochemistry* **36**, 12526-12534.
38. Studier, F.W. & Moffatt, B.A. (1986). Use of bacteriophage T7 RNA polymerase to direct selective high-level expression of cloned genes. *J. Mol. Biol.* **189**, 113-130.
39. Messerschmidt, A., & Pflugrath, J.W. (1987). Crystal orientation and X-ray pattern prediction routines for area detector diffractometer systems in macromolecular crystallography. *J. Appl. Crystallogr.* **20**, 306-315.
40. Sweet, R. M., & Skinner, J. (1995). An integrated graphical user interface for synchrotron beamline control and data collection. *American Crystallographic Association, Annual Meeting Abstracts* 1a.7.A 42.
41. Otwinowski, Z. & Minor, W. (1997). Processing of x-ray diffraction data collected in oscillation mode. *Methods Enzymol.* **276**, 307-326.
42. Ramakrishnan, V., & Biou, V. (1997). Treatment of multiwavelength anomalous diffraction data as a special case of multiple isomorphous replacement. *Methods Enzymol.* **276**, 538-556.
43. Sheldrick, G.H. (1991). Heavy atom location using SHELXS-90, in *Isomorphous Replacement and Anomalous Scattering*, Proceedings of the CCP4 Study Weekend 25-26 January, 1991. W. Wolf, P.R. Evans, & A.G.W. Leslie Eds., Daresbury Laboratory, Warrington WA4 4AD, England. pp. 23-38.
44. Terwilliger, T.C., Kim, S.-H., & Eisenberg, D. (1987). Generalized method of determining heavy-atom positions using the difference Patterson function. *Acta Crystallogr. A* **43**, 1-5.
45. Collaborative Computational Project, Number 4. The CCP4 Suite: programs for protein crystallography. (1994). *Acta Crystallogr. D* **50**, 760-763.
46. Otwinowski, Z. (1991). Maximum likelihood refinement of heavy atom parameters, In *Isomorphous Replacement and Anomalous Scattering*, (Wolf, W., Evans, P. R. & Leslie, A. G. W., eds), pp. 80-86, Daresbury Laboratory, Warrington, UK.
47. Cowtan, K. (1994). 'DM': an automated procedure for phase improvement by density modification. Joint CCP4 and ESF-EACBM Newsletter on Protein Crystallography **31**, 34-38.
48. Brünger, A.T. (1992). X-PLOR Version 3.1: a system for X-ray crystallography and NMR. Yale University Press, New Haven and London.
49. Brünger, A.T. (1992). Free R value: a novel statistical quantity for assessing the accuracy of crystal structures. *Nature* **355**, 472-475.
50. Kraulis, P.J. (1991). MolScript: a program to produce both detailed and schematic plots of protein structures. *J. Appl. Crystallogr.* **24**, 946-950.
51. Bacon, D.J. & Anderson, W.F. (1988). A fast algorithm for render space-filling molecule pictures. *J. Mol. Graph.* **6**, 219-220.
52. Merritt, E.A. & Murphy, M.E.P. (1994). Raster3D version 2.0. A program for photorealistic molecular graphics. *Acta Crystallogr. D* **50**, 869-873.